Pergamon

Scripta Materialia, Vol. 40, No. 10, pp. 1191–1198, 1999
Elsevier Science Ltd

1359-6462/99/$–see front matter

PII S1359-6462(99)00011-1

DETERMINATION OF ELASTOPLASTIC PROPERTIES BY INSTRUMENTED SHARP INDENTATION

A. E. Giannakopoulos and S. Suresh
Department of Materials Science and Engineering, Massachusetts Institute of Technology, Cambridge, MA 02139, USA

(Received November 25, 1998)
(Accepted in revised form January 8, 1999)

Introduction

Instrumented indentation methods, which provide a continuous record of the variation of indentation load, P, as a function of the depth of penetration, h, into the indented specimen, have been the topics of considerable attention in recent years. Such interest can be attributed to the following possible applications of the methods. (1) Properties such as Young's modulus, yield strength, and strain hardening exponent [1], as well as fracture toughness (e.g. [2]) of materials can be estimated by recourse to continuous indentation. (2) The magnitude and sign of any preexisting residual stresses can be assessed, in some cases, from indentation of surfaces [3]. (3) To the extent that continuum analyses adequately characterize indentation, the mechanical properties and residual stresses can be probed at different size scales by the appropriate choice of commercially available instrumentation, as well as indenter load, size and shape. (4) In materials with spatially varying composition, microstructure or dislocation density, the "inverse problem" of the determination of gradients in Young's modulus and yield strength can be accomplished, in some cases, by means of instrumented indentation (e.g. [4,5]).

Most of these applications of instrumented indentation are limited, however, by complications in clearly interpreting the indentation results. Such a complication arises from the "pile-up" or "sink-in" of the material around the indenter, which is primarily affected by the plastic properties of the material [6]. In a low-strain-hardening alloy, plastically displaced material tends to flow up to (and pile-up against) the faces of the indenter due to the incompressibility of plastic deformation. The result is a "barrel-shaped" impression due to pile-up around the sharp polygonal indenter, as shown in Fig. 1(a). On the other hand, for high-strain-hardening materials, the plastically deformed region is pushed out from the indenter with the imprint sinking below the initial surface level. The result is a "pin-cushion-like" impression around the sharp indenter, as shown in Fig. 1(b). Methods which properly account for pile-up or sink-in around the indenter are essential for the interpretation of the plastic properties of materials by recourse to instrumented indentation.

As a consequence of pile-up or sink-in, large differences may arise between the true contact area (which is influenced by the pile-up and sink-in of the materials and which is often difficult to assess *in-situ* during indentation) and the apparent contact area which is usually observed after indentation. A knowledge of the relationship between the indentation load and the true (projected) contact area, however, is essential to extract the mechanical properties from instrumented indentation. This difficulty can be overcome if explicit expressions, relating the true contact area A and the depth of penetration of the indenter h into the material being tested, are known *a priori* for different indenter geometries.

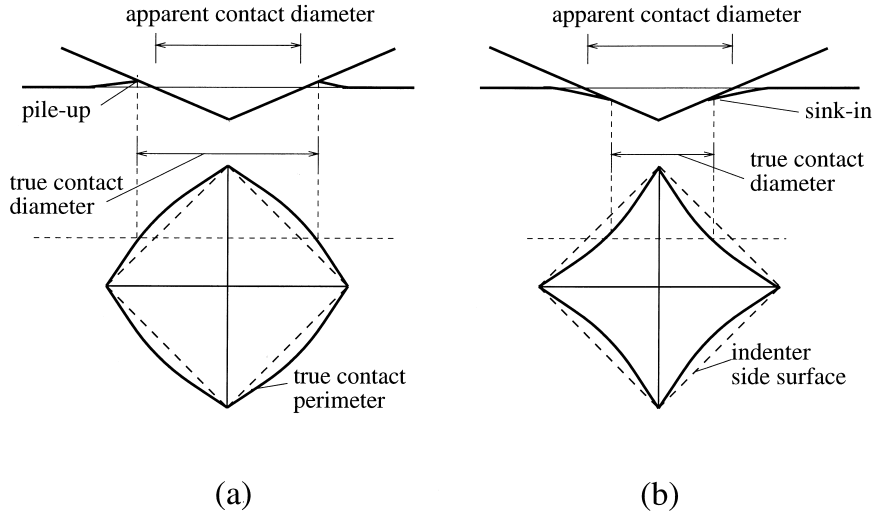

Figure 1. Schematic illustrations of (a) pile-up and (b) sink-in around a sharp indenter.

In this paper, we identify a general theoretical framework for instrumented sharp indentation and outline a methodology which enables the determination of elastic and plastic properties of materials by employing instrumented sharp (i.e. Vickers, Berkovich or conical) indentation. While prior analyses [6–8] address the "forward" problem of the mechanics of indentation, the present paper deals with the "inverse" problem of extracting material properties through instrumented indentation by utilizing the results of [6–8]. A key feature of the method outlined here is that it provides unique correlations between penetration depth h and true contact area A for commercially available sharp indenters; the method also circumvents the need for contact area measurement through visual observations while, at the same time, taking into account pile-up and sink-in. This paper also presents some new results on the equivalence between an energy approach and the displacement approach to indentation. When used in conjunction with the results reported in ref. [3], the method outlined here also facilitates the isolation of the effects of pre-existing residual stresses on sharp indentation response. Whereas attention is confined to sharp indentation in this paper, similar discussions for spherical indentation can be found elsewhere [9]. Details of the numerical simulations from which the present results are extracted are not reported here because of space restrictions; they can be found in refs. [4–6].

Keywords: Mechanical properties; Indentation; Hardness testing; Thin films; Non-destructive testing

A General Theoretical Framework for Sharp Indentation

Within the context of continuum analyses, sharp pyramidal or conical indenters lead to geometrically similar indentation states. That is, for a given indenter shape or included tip angle, the average contact pressure, $p_{av} = P/A$, is independent of the indentation load P or the true contact area A. It depends only on the included angle at the tip of the indenter (e.g. [3]). This average contact pressure is identified with the hardness H. Detailed three-dimensional, large-strain, plasticity simulations [6–8] reveal that the tip radius of the sharp indenter, R, has a negligible effect on indentation and the $P - h$ curve provided that the depth of penetration of the indenter into the material, $h > R/40$. In addition, adhesion and friction between the indenter and the substrate were found to have only a small effect on the hardness and the $P - h$ curve.

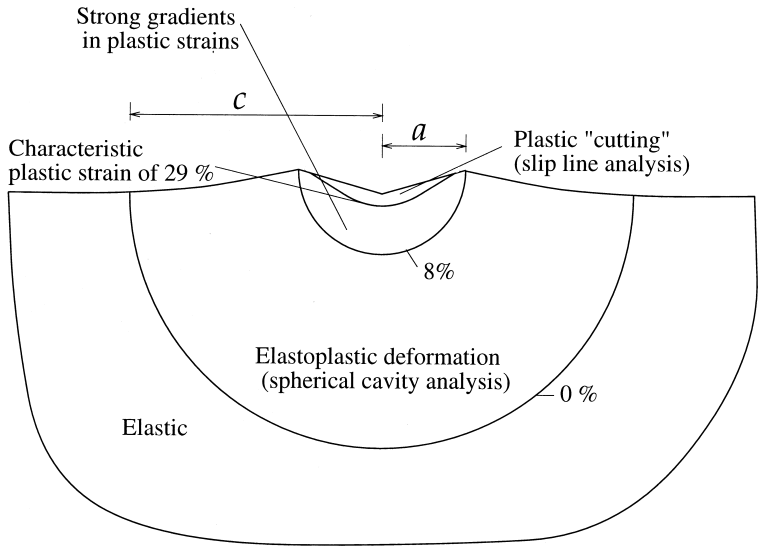

Figure 2. Different regimes of plastic flow at the tip of a sharp indenter.

Experiments [10] and computations [6] also show that there exists a unique characteristic equivalent plastic strain, which separates different modes of plastic deformation directly beneath the sharp indenter. This is schematically shown in Fig. 2. The innermost region comprises a zone where the material is "cut" by the sharp indenter; this cutting mode is amenable to analysis by means of the classical slip-line theories of rigid-perfect plasticity [11]. Surrounding this region is a zone of strong gradients in plastic strains which is engulfed by an elastoplastic regime where the so-called "cavity" model of Johnson [12] can be applied to extract the hemi-spherically shaped elastoplastic boundary. A unique characteristic strain separates the innermost "cutting" region from its surroundings. Although Tabor [13] proposed a value of 0.08 for this characteristic plastic strain, more elaborate studies [6,10] suggest a value in the range 0.25–0.36. In subsequent discussion, we use a fixed value of the characteristic strain of 0.29, which has been identified through finite element analyses of a wide range of ductile metals subjected to sharp indentation. The characteristic strain is independent of the indenter size or indentation load (provided that $h > R/40$), but is weakly influenced by the tip angle of the sharp indenter. Spherical or other blunt indenters do not lead to such a characteristic strain. Invoking the existence of this characteristic strain is a key step in the determination of mechanical properties and residual stresses by sharp indentation [3–6].

Force-Depth (P − h) Relations and the Displacement Approach

Figure 3 is a schematic of the load-penetration depth ($P - h$) curve for a sharp indenter. During loading, the curve generally follows the relation, $P = Ch^2$, where C is the indentation curvature which is a measure of the "resistance" of the material to indentation. The contact pressure, $p_{av} = P_{max}/A_{max}$, can be identified with the hardness of the indented material; P_{max} is the maximum indentation load which makes the indenter penetrate the material by a depth h_{max}, thereby creating a true (projected) contact area A_{max} on the indented surface. Three-dimensional finite-element simulations of elastoplastic indentation along with experiments [1,3–6] provide the following result:

$$C = \frac{P}{h^2} = M_1\sigma_{0.29}\left\{1 + \frac{\sigma_y}{\sigma_{0.29}}\right\}\left\{M_2 + \ln\left(\frac{E^*}{\sigma_y}\right)\right\}, \text{for } 0.5 \leq \frac{p_{av}}{\sigma_y} \leq 3.0. \quad (1)$$

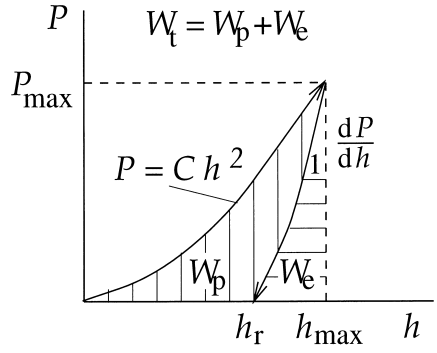

Figure 3. $P - h$ curves for loading and unloading, and the associated nomenclature.

In Eq. (1), σ_y is the yield strength and $\sigma_{0.29}$ is the stress corresponding to the characteristic plastic strain of 0.29 for the indented material in uniaxial compression, as shown schematically in Fig. 4. The constants in this equation are $M_1 = 7.143$ and $M_2 = -1$ for the Vickers pyramid indenter with an included tip angle of 136°. The corresponding values for the Berkovich indenter are $M_1 = 6.618$ and $M_2 = -0.875$ with an included tip angle of 130.6°. Circular conical indenters also follow the same results as the Vickers or Berkovich depending on the apex angle of the cone. If p_{av}/σ_y falls outside the bounds given in Eq. (1), the indentation response is either elastic (for $p_{av}/\sigma_y < 0.5$) or elastic-perfectly plastic (for $p_{av}/\sigma_y = 3$).

By accounting for the effects of strain hardening on pile-up and sink-in, and on the true contact area through three-dimensional simulations, the following relationship between A_{max} and h_{max} has been derived for elastoplastic materials [1,6]:

$$\frac{A_{max}}{h_{max}^2} = 9.96 - 12.64(1 - S) + 105.42(1 - S)^2 - 229.57(1 - S)^3 + 157.67(1 - S)^4, \text{ with } S = \frac{p_{av}}{E^*}. \quad (2)$$

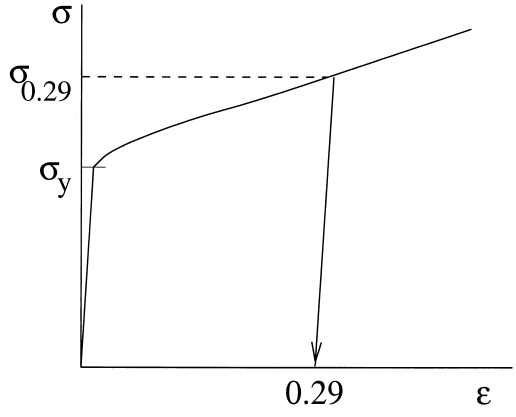

Figure 4. Uniaxial compression stress-strain curve and the characteristic strain.

TABLE 1
Numerically Determined Correlations Between Material Strain Hardening, Residual Impression Depth, and Maximum Contact Area.

$\{\sigma_{0.29} - \sigma_y\}/(0.29E^*) + 11\,\frac{\sigma y}{E^*}$	$(h_r/h_{max}) = (W_p/W_t)$	A_{max}/h^2_{max}
1	0.00	9.82
0.33	0.76	16.00
0.27	0.85	24.50
0.05	0.91	25.50
0.025	0.94	28.99
0.00	1.00	41.65

Note: (a) Pile-up occurs when $0.875 < (h_r/h_{max}) \leq 1$.
(b) Sink-in occurs when $0 \leq (h_r/h_{max}) < 0.875$.
(c) No pile-up or sink-in when $(h_r/h_{max}) = 0.875$, where the true contact area A and the apparent contact area A_{app} are equal, i.e. $A = A_{app} \approx 24.5h^2$ (for Vickers indentation).

This equation is a polynomial fit to the computationally determined values of A_{max}/h^2_{max}, which are listed in Table 1. More accurate analytical fits to the results can be obtained from the results of Table 1 by using higher order polynomials or other functional approximations. In Eq. (2), the effective elastic modulus of the indenter-specimen system, E^*, is defined as

$$E^* = \left[\frac{1-\nu^2}{E} + \frac{1-\nu_{in}^2}{E_{in}}\right]^{-1} = \frac{1}{c^*\sqrt{A_{max}}}\left(\frac{dP}{dh}\right), \tag{3}$$

where ν is Poisson's ratio, E is Young's modulus, the subscript 'in' denotes properties of the indenter, and dP/dh is the slope of the $P - h$ curve of the initial stages of unloading from P_{max} (see Fig. 3). The constant $c^* = 1.142$ for the Vickers pyramid indenter, 1.167 for the Berkovich indenter, and 1.128 for the circular conical indenter of any included apex angle.

The ratio of the residual depth of penetration, h_r upon complete unloading (see Fig. 3) to the maximum penetration depth, h_{max}, prior to unloading, is indicative of the extent of plastic deformation and strain hardening [4–6], such that

$$\frac{\sigma_{0.29} - \sigma_y}{0.29E^*} = 1 - 0.142\frac{h_r}{h_{max}} - 0.957\left(\frac{h_r}{h_{max}}\right)^2, \tag{4}$$

This result holds for Vickers, Berkovich as well as circular conical indenters. This equation, which is a polynomial fit to the computational results of Table 1, converges to the correct trends in the following two limiting cases. (1) For elastic indentation where $h_r = 0$, the right hand side of Eq. (4) obviously reduces to 1 indicating that $(\sigma_{0.29} - \sigma_y)/0.29 = E^*$ for linear elastic response. (2) For the case of a rigid-perfectly plastic material where $h_r = h_{max}$, the right hand side of Eq. (4) reduces to zero indicating no strain hardening. Different intermediate hardening responses during sharp indentation can be quantified with greater precision using the results shown in Table 1, and accounting for the influence of the initial yield strain, σ_y/E^*.

Elastoplastic finite element analyses of the sharp indenter, performed in the present study using numerical simulations similar to those reported in ref. [6], also reveal that

$$\frac{h_r}{h_{max}} = 1 - d^*\frac{p_{av}}{E^*} = 1 - d^*S, \tag{5}$$

where $d^* = 5$ for the Vickers pyramid indenter and $d^* = 4.678$ for the Berkovich indenter; the conical indenter has results similar to Vickers or Berkovich depending on the included apex angle. Equation (5)

is in reasonable accord with the empirical result of Breval and MacMillan [14] who employed Vickers indentation for a variety of materials. As shown in Table 1, $h_r/h_{max} = 0.875$ gives the critical strain hardening for which there is neither a pile-up nor a sink-in of the material around the indenter. Combining Eqs (2) and (5) readily provides a unique relationship between A_{max} and h_{max}, i.e., the true contact area which takes into account pile-up and sink-in can be extracted directly from the $P - h$ curve without the need for any visual observations.

Numerical simulations also reveal that the elastoplastic boundary underneath the sharp indenter in Fig. 2 has a hemi-spherical shape with radius, $c = \sqrt{(0.3P_{max})/\sigma_y}$. This result matches the experimentally based estimates of Zielinski et al. [15] who found that $c = \sqrt{(3P_{max})/(2\pi\sigma_y)}$. Johnson's cavity model [12] can sometimes significantly overestimate c.

The Energy Approach

From a practical standpoint, the measurement of residual depth h_r from instrumented indentation is generally prone to considerable experimental error due to a variety of factors, such as the roughness of the indented surface. As a result, the area under the $P - h$ curve, which provides a measure of elastic and plastic energy components of deformation during indentation, can be developed as an equivalent, but practically convenient, method for extracting mechanical properties. In this section, we demonstrate direct equivalence between the plastic energy of indentation and the residual depth, h_r.

The area under the loading portion of the $P - h$ curve is a measure of the total work, W_t, done by the indenter in deforming the material:

$$W_t = \int_0^{h_{max}} P(h)\mathrm{d}h = \int_0^{h_{max}} Ch^2\mathrm{d}h = \frac{Ch_{max}^3}{3} = \frac{P_{max}h_{max}}{3} = \frac{P_{max}^{1.5}}{3\sqrt{C}}. \tag{6}$$

Here, the commonly accepted notion that $P = Ch^2$ is invoked for the sharp indenter. As shown in Fig. 3, the total work W_t can be decomposed into elastic and plastic parts: $W_t = W_e + W_p$. Our computations reveal that

$$\frac{W_e}{W_t} = 1 - \frac{W_p}{W_t} = 1 - \frac{h_r}{h_{max}} = d^*\frac{p_{av}}{E^*} = d^*S. \tag{7}$$

This equation also suggests that the estimate of Stillwell and Tabor [16], namely $W_p/W_t = h_r/h_{max}$, for conical indenters also holds for sharp pyramidal indenters.

Experimental Comparison

The foregoing results on the equivalence between the displacement approach and the energy approach are validated here with the aid of available experimental evidence. For this purpose, use is made of the experiments reported in ref. [17] for the Berkovich indentation of a 1070 steel. The mechanical properties of this ultra-high-strength steel, derived from uniaxial tests, are: $E = 207$ GPa, $\nu = 0.3$, and $\sigma_y = 2.61$ GPa. The properties of the diamond pyramid indenter were taken as: $E_{in} = 900$ GPa and $\nu_{in} = 0.02$. From the first part of Eq. (3), $E^* = 182$ GPa. The hardness was quoted as $p_{av} = 9.5$ GPa. From the $P - h$ curves reported in ref. [17], the following values are extracted: $P_{max} = 100$ mN, $h_{max} = 0.733$ μm, $h_r = 0.567$ μm, $h_r/h_{max} = 0.773$, $\mathrm{d}P/\mathrm{d}h = 0.752$ MN/m (at the beginning of unloading), and $W_e = 7.725 \times 10^{-9}$ J.

First consider the predictions of the energy approach. From Eq. (6), $W_t = P_{max}h_{max}/3 = 24.433 \times 10^{-9}$ J. Thus, $W_e/W_t = 0.298$. Using $d^* = 4.678$, $p_{av} = 9.5$ GPa and $E^* = 182$ GPa, it is seen from Eq. (7) that $W_e/W_t = d^* p_{av}/E^* = 0.244$. Note also the result from Eq. (7) that $W_e/W_t = 1 - (h_r/h_{max}) = 1 - 0.773 = 0.227$.

Now consider the predictions of the displacement approach. Noting that $A_{max} = P_{max}/p_{av} = 10.53$ $(\mu m)^2$, $dP/dh = 0.752$ MN/m and $c^* = 1.167$, we predict that $E^* = 198.6$ GPa. From Table 1, estimate A_{max} to be 8.92 $(\mu m)^2$. Thus, some features of the proposed analysis are validated by experiments on the 1070 steel, although a more complete comparison of the predictions of the plastic response with experiments could not be made from the information provided ref. [17].

A Step-by-Step Method for Sharp Indentation Tests

With the above theoretical framework, we now present a step-by-step method for the estimation of local and bulk mechanical properties. A notable feature of this method (described in [1]) is that properties such as Young's modulus, compressive yield strength, strain hardening exponent, strength at a plastic strain of 0.29 and hardness can be determined *in situ* from an automated recording of $P - h$ curves. The method circumvents, by design, the need for visual observations of the contact area and incorporates into the analysis the effects of pile-up and sink-in.

This method is expected to be valid provided that the diameter of the impression made by the indenter spans at least five grains (which is the limitation of the continuum analysis employed). For thin films on substrates, it must additionally be ensured that the contact diameter is typically smaller than about one third of the film thickness in order that the indentation response is not influenced by the substrate.

The present problem of property determination has four unknowns: E, σ_y, $\sigma_{0.29}$, and p_{av} (which is the hardness). A complete instrumented indentation $P - h$ curve obtained during loading and full unloading gives the following four parameters: the loading curvature $C = P_{max}/h_{max}^2$, the initial unloading slope dP/dh, the maximum indentation depth h_{max} and the residual depth of penetration, h_r. (Since $h_r/h_{max} = W_p/W_t$, a knowledge of the ratio of plastic work to total work from the area under the indentation curve may also suffice instead of h_r/h_{max}.) The problem is thus fully determinate. The proposed method involves the following steps.

1: Experimentally determine the $P - h$ curve, during complete loading and unloading, for the material whose properties are to be determined. Use a Vickers, Berkovich or conical indenter (whose apex angle is the same as that of Vickers or Berkovich).
2: From the $P - h$ curve, identify h_r and h_{max} and calculate h_r/h_{max}.
3: Using this value of h_r/h_{max}, find $S = p_{av}/E^*$ from Eq. (5). Alternatively, estimate the ratio of the elastic work to total work, W_e/W_t, graphically from the $P - h$ curve, apply Eq. (7) and find S.
4: With S so determined, and h_{max} directly observed from the $P - h$ curve, and obtain the true contact area at maximum load, A_{max}, from Eq. (2) or Table 1.
5: Obtain E_{in} and ν_{in} for the indenter material directly from the manufacturer or from standard data tables available from the literature. If Young's modulus, E, and Poisson's ratio, ν, of the indented material are known, compute E^* from Eq. (3). Use the value of p_{av}/E^* found in Step 3 and calculate p_{av}. If the elastic properties of the indenter and the indented material are not known *a priori*, determine the initial unloading slope dP/dh as shown in Fig. 3, use A_{max} from Step 4, and calculate E^* using the second part of Eq. (3).
6: Using the value of h_r/h_{max} found in Step 2, and E^* from Step 5, use Eq. (4) or Table 1 and find the quantity $(\sigma_{0.29} - \sigma_y)$.

7: With P_{max} and h_{max} identified from the $P - h$ curve, use the relation $P_{max} \approx Ch^2_{max}$, and estimate C using least-square fit. With this value of C and $(\sigma_{0.29} - \sigma_y)$ from Step 6, iterate Eq. (1) and estimate σ_y and $\sigma_{0.29}$.
8: Calculate the strain hardening exponent $n \approx \ln \{\sigma_{0.29} - \ln (\sigma_y)\}/5$.

Acknowledgements

The preparation of this manuscript was supported by the MRSEC program of National Science Foundation under Grant No. DMR 9632570, which is funded at MIT through a subcontract from the State University of New York at Stony Brook.

References

1. S. Suresh, J. Alcala, and A. E. Giannakopoulos, MIT Case No. 7280, Massachusetts Institute of Technology (1996). Patent application pending.
2. B. R. Lawn, Fracture of Brittle Solids, 2nd edn., Cambridge University Press, Cambridge, UK (1993).
3. S. Suresh and A. E. Giannakopoulos, Acta Mater. 46, 5755 (1998).
4. S. Suresh, A. E. Giannakopoulos, and J. Alcala, Acta Mater. 45, 1307 (1997).
5. S. Suresh and A. E. Giannakopoulos, Report Inst-2/98, Massachusetts Institute of Technology (1998).
6. A. E. Giannakopoulos, P.-L. Larson, and R. Vestergaard, Int. J. Solids Struct. 31, 2679 (1994).
7. A. E. Giannakopoulos and P.-L. Larson, Mech. Mater. 25, 1 (1997).
8. P.-L. Larson, A. E. Giannakopoulos, E. Soderlund, D. J. Rowcliffe, and R. Vestergaard, Int. J. Solids Struct. 33, 221 (1996).
9. J. Alcala, A. E. Giannakopoulos, and S. Suresh, J. Mater. Res. 13, 1390 (1998).
10. M. M. Chaudhri, Acta Mater. 46, 3047 (1998).
11. F. J. Lockett, J. Mech. Phys. Solids. 11, 345 (1963).
12. K. L. Johnson, J. Mech. Phys. Solids. 18, 115 (1970).
13. D. Tabor, Hardness of Metals, Clarendon Press, Oxford, UK (1951).
14. E. Breval and N. H. MacMillan, J. Mater. Sci. Lett. 4, 741 (1985).
15. W. Zielinski, H. Huang, and W. W. Gerberich, J. Mater. Res. 8, 1300 (1993).
16. N. A. Stillwell and D. Tabor, Proc. Phys. Soc. 78, 169 (1961).
17. S. Jayaraman, G. T. Hahn, W. C. Oliver, C. A. Rubin and P. C. Bastias, Int. J. Solids Struct. 35, 365 (1998).